

# Thermoelectric effects of quantum dot arrays embedded in nanowires

Yen-Chun Tseng<sup>1</sup>, David M.-T. Kuo<sup>1,2,†</sup>, Yia-Chung Chang<sup>3,4,\*</sup> and Chia-Wei Tsai<sup>1</sup>

<sup>1</sup>*Department of Electrical Engineering and* <sup>2</sup>*Department of Physics,*

*National Central University, Chungli, 32001 Taiwan and*

*<sup>3</sup>Research Center for Applied Science, Academic Sinica,*

*Taipei, 11529, Taiwan and* <sup>4</sup>*Department of Physics,*

*National Cheng-Kung University, Tainan, 70101, Taiwan*

(Dated: January 12, 2021)

The thermoelectric properties of quantum dot arrays (QDAs) embedded in nanowires connected to electrodes are studied theoretically in the Coulomb blockade regime. A Hubbard-Anderson model is used to simulate the electronic contribution to thermoelectric properties of a QDA junction system. The electrical conductance, Seebeck coefficient, and electron thermal conductance are calculated by both the Keldysh Green function method and the mean-field approach. The phonon thermal conductivities are calculated by using the equation of phonon radiative transfer method. In the Coulomb blockade regime the electron thermal conductance is much smaller than the phonon thermal conductance. Therefore, the optimal figure of merit ( $ZT$ ) can be enhanced by increasing thermal power and decreasing phonon thermal conductance simultaneously. We found that it is possible to obtain  $ZT$  value of InGaAs/GaAs QDAs embedded in nanowires larger than one at room temperature.

## I. INTRODUCTION

Recently, many efforts have been devoted to seeking efficient thermoelectric (TE) materials with the figure of merit ( $ZT$ ) larger than 3, because there are potential applications of solid state thermal devices such as coolers and power generators, which can replace conventional compressor-based refrigerators and fossil fuel generators to reduce  $CO_2$  emission [1-7]. Nevertheless, the optimization of TE materials is extremely difficult, since  $ZT = S^2 G_e T / \kappa$  depends on the electrical conductance ( $G_e$ ), Seebeck coefficient ( $S$ ), and thermal conductance ( $\kappa$ ).  $T$  is the equilibrium temperature. These physical quantities are usually related to one another. Mechanisms leading to the enhancement of power factor ( $PF = S^2 G_e$ ) would also enhance the thermal conductance. Consequently, it is difficult to obtain  $ZT$  above one in conventional bulk materials.[1]

Impressive  $ZT$  values for quantum dot array (QDA) embedded in nanowires have been experimentally demonstrated.[8] The power factor and thermal conductance become independent thermoelectric variables under the condition  $\kappa_e / \kappa_{La} \ll 1$ , where  $\kappa_e$  and  $\kappa_{La}$  denote, respectively, the electron thermal conductance and lattice thermal conductance.[8] In the Coulomb blockade regime, electron transport process is seriously suppressed by the electron Coulomb interactions, therefore  $\kappa_e$  as well as  $G_e$  are reduced significantly.[9] Under the condition  $\kappa_e / \kappa_{La} \ll 1$ , one can increase the power factor and decrease the phonon thermal conductance simultaneously to optimize  $ZT$ .[9]

Thermoelectric properties of quantum dots (QDs) embedded in a matrix connected to metallic electrodes were studied by several groups in the absence of phonon thermal conductivity.[10-16] For the applications of solid state coolers and power generators at room temperature, one needs to consider a large number of serially coupled

QDs, otherwise it is not easy to maintain a large temperature difference across the QD junction, which was pointed out to be crucial in the implementation of high-efficiency thermoelectric devices.[1,2] In addition, the phonon thermal conductivity plays a significant role in the optimization of  $ZT$  at high temperatures. In this paper, we carry out theoretical analysis of  $ZT$  of QD arrays embedded in nanowires, including the phonon conductance, which is calculated by using the phonon radiative transfer method as introduced in Ref. [17]. Although the method does not take into account the microscopic mechanisms associated with quantum confinement of acoustic phonons, it gives reasonable agreement with the lattice-dynamics model and experiments for nanowires by merely considering the boundary scattering effect of phonons.

## II. FORMALISM

A QDA embedded in a nanowire connected to the metallic electrodes can be described by the Hubbard-Anderson model. Here we consider nanoscale semiconductor QDs, in which the energy level separations are much larger than their on-site Coulomb interactions and thermal energies. Thus, only one energy level for each quantum dot needs to be considered. The Hamiltonian of the system is given by  $H = H_0 + H_{QD}$ :

$$H_0 = \sum_{k,\sigma} \epsilon_k a_{k,\sigma}^\dagger a_{k,\sigma} + \sum_{k,\sigma} \epsilon_k b_{k,\sigma}^\dagger b_{k,\sigma} \quad (1)$$

$$+ \sum_{k,\sigma} V_{k,L} d_{L,\sigma}^\dagger a_{k,\sigma} + \sum_{k,\sigma} V_{k,R} d_{R,\sigma}^\dagger b_{k,\sigma} + c.c$$

where the first two terms describe the free electron gas of left and right electrodes.  $a_{k,\sigma}^\dagger$  ( $b_{k,\sigma}^\dagger$ ) creates an electron of momentum  $k$  and spin  $\sigma$  with energy  $\epsilon_k$  in the left (right)

electrode.  $V_{k,\ell}$  ( $\ell = L, R$ ) describes the coupling between the electrodes and the left (right) QD.  $d_{\ell,\sigma}^\dagger$  ( $d_{\ell,\sigma}$ ) creates (destroys) an electron in the  $\ell$ -th dot.

$$H_{QD} = \sum_{\ell,\sigma} E_\ell n_{\ell,\sigma} + \sum_\ell U_\ell n_{\ell,\sigma} n_{\ell,\bar{\sigma}} \quad (2)$$

$$+ \frac{1}{2} \sum_{\ell,j,\sigma,\sigma'} U_{\ell,j} n_{\ell,\sigma} n_{j,\sigma'} + \sum_{\ell,j,\sigma} t_{\ell,j} d_{\ell,\sigma}^\dagger d_{j,\sigma},$$

where  $E_\ell$  is the spin-independent QD energy level, and  $n_{\ell,\sigma} = d_{\ell,\sigma}^\dagger d_{\ell,\sigma}$ .  $U_\ell$  and  $U_{\ell,j}$  describe the intradot and interdot Coulomb interactions, respectively.  $t_{\ell,j}$  describes the electron interdot hopping. Note that the interdot Coulomb interactions as well as intradot Coulomb interactions play a significant role on the charge transport for semiconductor QD array.

Using the Keldysh-Green's function technique [18], the charge and heat currents of electrons leaving electrodes are expressed as

$$J = \frac{2e}{h} \int d\epsilon \mathcal{T}(\epsilon) [f_L(\epsilon) - f_R(\epsilon)], \quad (3)$$

$$Q_{L(R)} = \pm \frac{2}{h} \int d\epsilon \mathcal{T}(\epsilon) (\epsilon - \mu_{L(R)}) [f_L(\epsilon) - f_R(\epsilon)], \quad (4)$$

where  $\mathcal{T}(\epsilon)$  is the transmission coefficient.  $f_{L(R)}(\epsilon) = 1/[e^{(\epsilon - \mu_{L(R)})/k_B T_{L(R)}} + 1]$  denotes the Fermi distribution function for the left (right) electrode.  $\mu_L$  and  $\mu_R$  denote the chemical potentials of the left and right leads, respectively, with their average denoted by  $E_F = (\mu_L + \mu_R)/2$ .  $(\mu_L - \mu_R) = e\Delta V$  is the voltage across the QDA junction.  $T_{L(R)}$  denotes the equilibrium temperature of the left (right) electrode.  $e$  and  $h$  denote the electron charge and Planck's constant, respectively.  $Q_{L(R)}$  denotes the heat current leaving from the left (right) electrode.

In the linear response regime, Eqs. (3) and (4) can be rewritten as

$$J = \mathcal{L}_{11} \frac{\Delta V}{T} + \mathcal{L}_{12} \frac{\Delta T}{T^2} \quad (5)$$

$$Q = \mathcal{L}_{21} \frac{\Delta V}{T} + \mathcal{L}_{22} \frac{\Delta T}{T^2}, \quad (6)$$

where there are two sources of driving force to yield the charge and heat currents.  $\Delta T = T_L - T_R$  is the temperature difference across the junction. The thermoelectric coefficients in Eqs. (5) and (6) ( $\mathcal{L}_{11}$ ,  $\mathcal{L}_{12}$ ,  $\mathcal{L}_{21}$ , and  $\mathcal{L}_{22}$ ) are evaluated by

$$\mathcal{L}_{11} = \frac{2e^2 T}{h} \int d\epsilon \mathcal{T}(\epsilon) \left( \frac{\partial f(\epsilon)}{\partial E_F} \right)_T, \quad (7)$$

$$\mathcal{L}_{12} = \frac{2eT^2}{h} \int d\epsilon \mathcal{T}(\epsilon) \left( \frac{\partial f(\epsilon)}{\partial T} \right)_{E_F}, \quad (8)$$

$$\mathcal{L}_{21} = \frac{2eT}{h} \int d\epsilon \mathcal{T}(\epsilon) (\epsilon - E_F) \left( \frac{\partial f(\epsilon)}{\partial E_F} \right)_T, \quad (9)$$

and

$$\mathcal{L}_{22} = \frac{2T^2}{h} \int d\epsilon \mathcal{T}(\epsilon) (\epsilon - E_F) \left( \frac{\partial f(\epsilon)}{\partial T} \right)_{E_F}. \quad (10)$$

Here  $\mathcal{T}(\epsilon)$  and  $f(\epsilon) = 1/[e^{(\epsilon - E_F)/k_B T} + 1]$  are evaluated under the equilibrium condition. The detailed expression of  $\mathcal{T}(\epsilon)$  can be found in Ref. [19].

If the system is in an open circuit, the electrochemical potential will be established in response to a temperature gradient; this electrochemical potential is known as the Seebeck voltage (Seebeck effect). The Seebeck coefficient (amount of voltage generated per unit temperature gradient) is defined as  $S = \Delta V/\Delta T = -\mathcal{L}_{12}/(T\mathcal{L}_{11})$ . To judge whether the system is able to generate or extract heat efficiently, we need to consider the figure of merit [1]

$$ZT = \frac{S^2 G_e T}{\kappa_e + \kappa_{La}} \equiv \frac{(ZT)_0}{1 + \kappa_{La}/\kappa_e}. \quad (11)$$

Here,  $G_e = \mathcal{L}_{11}/T$  is the electrical conductance and  $\kappa_e = ((\mathcal{L}_{22}/T^2) - S^2 G_e T)$  is the electron thermal conductance.  $(ZT)_0$  represents the  $ZT$  value in the absence of phonon thermal conductance,  $\kappa_{La}$ . In the Hamiltonian  $H$ , the term  $(H_{e,ph})$  describing the interactions between electrons and phonons is ignored. For simplicity, we adopt  $\kappa_{La} = \kappa_{wire} F_s$  to describe the phonon thermal conductance of QDA embedded a nanowire. The dimensionless scattering factor  $F_s$  is used to include the phonon scattering effect arising from surface boundary of QDs.[1] It is possible to reduce phonon thermal conductance by one order of magnitude when QDs in a quantum wire behave like phonon scatterers.[20] Therefore, the maximum  $F_s$  is assumed to be 0.1 in this study. For example, Ref. [20] pointed out that the phonon thermal conductance reduction of QDA nanowires in a high temperature regime arises from the filtering of high frequency phonons.[2] However, the method considered in Ref. [20] requires a heavily numerical calculation of  $\kappa_{La}$  in the optimization of  $ZT$ .

Based on Holland's model [21,22] in which the longitudinal and transverse acoustical phonon branches are treated separately, we calculate  $\kappa_{wire}$  of a rectangular nanowire with cross sectional area  $A$  and length  $L_x$ . The thermal conductance  $\kappa_{wire}$  is related to the phonon thermal conductivity by  $\kappa_{wire} = \kappa_{ph} A/L_x$ , where  $\kappa_{ph} = K_0 + K_{Tu} + K_L$  denotes the thermal conductivity with

$$K_{T0} = \frac{2}{3} T^3 \int_0^{\theta_1/T} \frac{C_{T0} x^4 e^x (e^x - 1)^{-2} dx}{\tau_b^{-1} + \tau_I^{-1} + \beta_T x T^5}, \quad (12)$$

$$K_{Tu} = \frac{2}{3} T^3 \int_{\theta_1/T}^{\theta_2/T} \frac{C_{Tu} x^4 e^x (e^x - 1)^{-2} dx}{\tau_b^{-1} + \tau_I^{-1} + \beta_{Tu} x^2 T^2 / \sinh(x)}, \quad (13)$$

and

$$K_L = \frac{1}{3} T^3 \int_0^{\theta_3/T} \frac{C_L x^4 e^x (e^x - 1)^{-2} dx}{\tau_b^{-1} + \tau_I^{-1} + \beta_L x^2 T^5}. \quad (14)$$

The phonon thermal conductivities  $K_{T_0}$ ,  $K_{Tu}$ , and  $K_L$  result from the low-frequency transverse branch, high-frequency transverse branch, and longitudinal acoustical phonon branch, respectively. In Eqs. (12)-(14), we have  $C_{j=T_0,Tu,L} = (k_B/2\pi^2 v_j)(k_B/\hbar)^3$ , where  $v_j$  is the phonon group velocity for the  $j^{th}$ -branch.  $\tau_b^{-1}$  is the phonon boundary scattering rate, and  $\tau_I^{-1} = \alpha x^4 T^4$  is the phonon-impurity scattering rate.  $\beta_T x T^5$ ,  $\beta_{Tu} x^2 T^2 / \sinh(x)$ , and  $\beta_L x^2 T^5$  arise from three-phonon scattering rates.  $\alpha$  and  $\beta_j$  are empirical parameters determined by fitting experimental data.  $\theta_i(\hbar\omega_i/k_B)$  ( $i = 1, 2$ , and  $3$ ) denotes the Debye temperature. The frequencies of  $\omega_i$ , for  $T_0$ ,  $Tu$  and  $L$  modes can be found in Ref. [17]. The  $\alpha$ ,  $\beta_j$ ,  $v_j$  and  $\theta_i$  parameters for Si and GaAs are adopted from Refs. [17] and [22], respectively. Eqs. (12)-(14) can well describe the phonon thermal conductivity of semiconductor materials with  $\tau_b = v_b/L$ .  $v_b = [(2v_T^{-1} + v_L^{-1})/3]^{-1}$  is the average phonon group velocity, where  $v_T$  and  $v_L$  correspond to the group velocities of the transverse and longitudinal branches.  $L$  denotes the sample size. Chen and Tien [21] extended the Holland model to illustrate the phonon thermal conductivity of quantum wells by considering the geometry effect on  $\tau_b$ . Based on the formalism of ref.[21], the phonon-boundary scattering rate ( $\tau_b^{-1}$ ) of quantum wire is derived and determined by

$$\tau_b^{-1} = (1/\mathcal{G} - 1) \cdot \tau_t^{-1}, \quad (15)$$

where  $\tau_t = (A\omega^4 + (B_1 + B_2)T^3\omega^2 + v_b/L_c)^{-1}$  is the total internal relaxation time of the bulk which includes normal process and umklapp process.  $A = \alpha(\hbar/k_B)^4$ , and  $B_j = \beta_j(\hbar/k_B)^2$ .  $L_c$  denotes the sample length. The factor of  $\mathcal{G} = \mathcal{G}^{++} + \mathcal{G}^{+-} + \mathcal{G}^{-+} + \mathcal{G}^{--}$  illustrates the boundary effects on the phonon thermal conductivity of nanowires. The expression of  $\mathcal{G}$  is given by

(i)  $0 < \theta < \pi/2$  and  $0 < \phi < \pi$

$$\mathcal{G}^{++}/\Pi = \int d\Omega \frac{(e^{-\xi_y} - 1)(e^{-\xi_z} - 1)}{e^{-\xi_y} e^{-\xi_z} - 1}, \quad (16)$$

(ii)  $0 < \theta < \pi/2$  and  $\pi < \phi < 2\pi$

$$\mathcal{G}^{+-}/\Pi = \int d\Omega \frac{(e^{-\xi_y} - 1)(e^{-\xi_z} - 1)}{e^{-\xi_y} e^{-\xi_z} - 1}, \quad (17)$$

(iii)  $\pi/2 < \theta < \pi$  and  $0 < \phi < \pi$

$$\mathcal{G}^{-+}/\Pi = \int d\Omega \frac{(e^{-\xi_y} - 1)(e^{-\xi_z} - 1)}{e^{-\xi_y} e^{-\xi_z} - 1}, \quad (18)$$

(iv)  $\pi/2 < \theta < \pi$  and  $\pi < \phi < 2\pi$

$$\mathcal{G}^{--}/\Pi = \int d\Omega \frac{(e^{-\xi_y} - 1)(e^{-\xi_z} - 1)}{e^{-\xi_y} e^{-\xi_z} - 1}. \quad (19)$$

We have the notations  $\Pi = \frac{3}{4\pi L_y L_z}$  and  $d\Omega = dy dz d\theta d\phi \sin^3(\theta) \cos^2(\phi)$  in Eqs. (16)-(19), where  $L_{y(z)}$

is the lateral size of rectangular wire in the  $y(z)$  direction. The other notations are  $\xi_y = -y/(\Lambda \sin(\theta) \sin(\phi))$ ,  $\xi_z = -z/(\Lambda \cos(\theta))$ ,  $\xi_y = (L_y - y)/(\Lambda \sin(\theta) \sin(\phi))$  and  $\xi_z = (L_z - z)/(\Lambda \cos(\theta))$ . The average phonon mean free path is assumed to be  $\Lambda = v_b \tau_t$ .

The phonon thermal conductivities ( $\kappa_{ph}$ ) of rectangular Si and GaAs nanowires calculated by using Eqs. (12)-(14) are plotted for two different topological structures in Fig. 1. The calculations of silicon nanowire can be used to compare with experimental results to examine the validity of the scheme adopted in Ref. [21]. The heat problem of high efficiency solar cells made of III-V compounds (such as GaAs) can degrade the system performance.[1] Thus, it is important to design a GaAs cooler, which can be integrated with the solar cell to solve such a problem. Figure 1(a) shows  $\kappa_{ph}$  of Si nanowire with  $L_y = L_z$  as a function of temperature for three cross-section areas: solid line ( $A = (30 \text{ nm})^2$ ), dashed-dotted line ( $A = (10 \text{ nm})^2$ ) and dashed line ( $A = (5 \text{ nm})^2$ ). It is expected that  $\kappa_{ph}$  decreases with decreasing cross-section area due to enhanced boundary scattering. For a nanowire with small cross section,  $\kappa_{ph}$  increases slower with respect to  $k_B T$  for  $T > 200 \text{ K}$ . These results are consistent with other theoretical calculations [23] and experimental observations.[24,25] For nanowires with large cross section, however,  $\kappa_{ph}$  is slightly underestimated compared to other theoretical works.[23] For the smallest area considered ( $A = (5 \text{ nm})^2$ ), the  $\kappa_{ph}$  value obtained is very close to the result calculated from the lattice-dynamics model in Ref. 20, which takes into account the quantum confinement of acoustic phonons. Although a nanowire with even smaller cross section leads to much smaller phonon thermal conductivity, it is a challenge to implement such tiny nanowires.[1,2]

Figure 1(b) shows  $\kappa_{ph}$  of GaAs nanowire as a function of temperature for different  $L_z$  sizes with  $L_y$  fixed at  $5 \text{ nm}$ . We note that  $\kappa_{ph}$  of GaAs is smaller than that of Si in a wide temperature range for  $A = (5 \text{ nm})^2$  because the average group velocity in GaAs is smaller.  $\kappa_{ph}$  increases with increasing  $L_z$ . However,  $\kappa_{ph}$  for  $L_z = 500 \text{ nm}$  becomes almost the same as  $\kappa_{ph}$  of GaAs thin film with  $L_z = L_c = 0.729 \text{ cm}$  and  $L_y = 5 \text{ nm}$  (see the solid and black line). This implies that the size effect of  $L_z$  on  $\kappa_{ph}$  can be ignored when  $L_z$  is larger than  $500 \text{ nm}$ , **comparable to** the average phonon mean free path of GaAs. The maximum  $\kappa_{ph}$  value of GaAs thin film at  $T = 100 \text{ K}$  is around  $4 \text{ W/mK}$ , which is still smaller than that of Si nanowire with  $A = (10 \text{ nm})^2$ . This implies that GaAs may have a better  $ZT$  value than silicon at room temperature. Our results for GaAs are consistent with the calculation of Ref. [26]. Although the TE properties of germanium/silicon QDs system are interesting for their low cost fabrication process [27], the silicon semiconductor TE devices can not be directly integrated with III-V compound solar cell systems.[1] Therefore, we focus on the  $ZT$  optimization of InGaAs/GaAs QDs junction system in the next section.

### III. RESULTS AND DISCUSSION

Because it is important to reduce the phonon thermal conductivity in the optimization of  $ZT$ , we need to consider a QDA nanowire with long length. Therefore, before investigating the TE properties of QDAs with large number of coupled dots, we first consider the simplest structure of QDA, which consists of serially coupled triple QDs (SCTQD). Although we have theoretically studied the transport and TE properties of triple QD molecules with full solution in the Coulomb blockade regime,[28,29] it is still a challenging work to obtain the full solution to the charge transport through QDAs with more than three dots due to the fact that the calculation scales up exponentially. To solve such a difficult problem many efforts which adopt some approximation schemes were attempted.[9,30-32] The Hartree-Fock approximation (HFA) is often used to investigate the TE coefficients of realistic molecules.[30-32] As a consequence, it is desirable to examine the validity of such a mean-field approach. At high temperatures, in the absence of interdot Coulomb interactions the results based on the approach of Ref. [9] can achieve good agreement with those calculated by the full solution as reported in Ref. [29]. Therefore, we can examine the validity of HFA method by using the approach of Ref.[9] instead of using the full solution of Ref. [29], which requires much heavier numerical calculation. In addition, the approximation of Ref. [9] can provide a closed form transmission coefficient of Eqs. (7)-(10), which is useful for analyzing the charge transport properties.

Because the optimization of power factor (PF) favors identical QDs, size-independent electron hopping strength, and symmetrical tunneling rates,[9] in Fig. 2 we plot  $G_e$ ,  $S$ ,  $\kappa_e$  and  $PF$  of SCTQD as functions of gate voltage ( $eV_g$ ) at two different temperatures by considering  $t_{\ell,j} = t_c = 3\Gamma_0$ ,  $U_\ell = U_0 = 30\Gamma_0$  and symmetrical tunneling rates ( $\Gamma_L = \Gamma_R = 1\Gamma_0$ ). All energy scales are in units of  $\Gamma_0$ , which is taken to be 1 meV. Here, the interdot Coulomb interactions are ignored for simplicity when we examine the validity of HFA method. The solid lines and dot-dashed lines are calculated according to the procedure of Ref.[9] and the HFA method of Ref.[30-32], respectively. The approach of Ref. [9], which neglects the interdot Coulomb interactions, is called the on-site Coulomb approximation (OCA). Both OCA and HFA are efficient tools for studying the charge transport through molecular junctions.

For all four physical quantities ( $G_e$ ,  $S$ ,  $\kappa_e$  and  $PF = S^2 G_e$ ), the spectra consist two main groups of features, which are mirror image of each other with respect to the mid point ( $eV_g = 45\Gamma_0$ ). This is a consequence of the electron-hole symmetry possessed by the SCTQD structures in the absence of interdot Coulomb interactions [29]. At low temperature ( $k_B T = 0.1\Gamma_0$ ), there is a gap between the two groups, which is related to on-site Coulomb interaction,  $U_0$ . The first three peaks of  $G_e$  (shown by the solid line) correspond to three reso-

nant channels at  $E_0 - \sqrt{2}t_c$ ,  $E_0$ , and  $E_0 + \sqrt{2}t_c$ . For the higher-energy group, there are also three peaks arising from resonant channels at  $E_0 + U_0 - \sqrt{2}t_c$ ,  $E_0 + U_0$  and  $E_c + U_0 + \sqrt{2}t_c$ . We find that the behaviors of  $G_e$ ,  $S$  and  $\kappa_e$  calculated by HFA (dot-dashed lines) are quite different from those calculated by OCA (solid lines). For example, the maximum  $G_e$  of dot-dashed lines is larger than  $e^2/h$  (quantum conductance), but not for OCA. This is due to the inability of HFA to include electron correlation. The energy positions of resonant channels within HFA depend on the average occupation number in each QD.[30-32], which can be a fractional number. In contrast, within OCA the energy positions of resonant channels are determined by integer charges, while electron correlation functions and fractional occupation numbers only appear in the probability weights of quantum paths.[9] In addition, we observe an unphysical enhancement of  $S$  in the middle of the Coulomb gap ( $eV_g = 45\Gamma_0$ ) for HFA results (dot-dashed line). This illustrates the drawback of HFA calculation for TE coefficients of QDs at low temperatures when the charging process plays a significant role. At high temperatures (for example,  $k_B T = 10\Gamma_0$ ), the detailed resonant structures are washed out, and the unphysical enhancement of  $S$  in the middle of the Coulomb gap also disappears. These two approaches give qualitatively similar results at high temperatures. However, the HFA approach tends to overestimate  $G_e$ ,  $\kappa_e$ , and  $PF$ . If we include the interdot Coulomb interactions, the interdot correlation effects become crucial[29]. **The symmetrical behavior of TE coefficients will be lost.** In general, we will obtain smaller PF for QD energy levels below  $E_F$  than that for QD energy levels above  $E_F$ .[9,29] This indicates that to achieve maximum PF, it is preferable to have the orbital depletion situation with the total occupation number  $N = \sum_\sigma (N_{L,\sigma} + N_{C,\sigma} + N_{R,\sigma}) \leq 1$ , where  $N_{\ell,\sigma}$  denotes the single particle occupation number in dot  $\ell$ .[29]

For TE devices operated at room temperature, it is important to optimize their  $ZT$  values at high temperatures. To further clarify the differences between these two approaches, Fig. 3 shows  $G_e$ ,  $S$ ,  $\kappa_e$  and  $PF$  as functions of the detuning energy ( $\Delta = E_0 - E_F > 0$ ) at various temperatures. **Note that in Fig. 3, we consider the case with QD energy levels above  $E_F$ , which satisfies the condition for orbital depletion.** In one-particle transport process (QD molecule with an empty state) **only the intradot Coulomb interaction effects are important**.[29] This is a typical feature for carrier transport in the Coulomb blockade regime.[9] The other physical parameters are the same as those of Fig. 2. From the results of  $S$  and  $PF$ , these two approaches agree well with each other when QD energy levels are far above  $E_F$ . This is expected, because the electron Coulomb interactions become unimportant for large  $\Delta$  values. The maximum PF value decreases with increasing temperature. For  $k_B T = 1\Gamma_0$ ,  $k_B T = 5\Gamma_0$  and  $k_B T = 13\Gamma_0$ , the maximum  $PF$  occurs at near  $\Delta = 5\Gamma_0$ ,  $\Delta = 15\Gamma_0$ , and  $\Delta = 35\Gamma_0$ , respectively. When  $k_B T = 26\Gamma_0$ , the

maximum PF occurs at near  $\Delta = 50\Gamma_0$ .

From results of Fig. 3, we see that HFA is a reasonably good approximation for analyzing the TE coefficients of QDAs with QD energy levels above  $E_F$ . Thus, we can use HFA to investigate TE coefficients of QDA nanowire with large number of dots. Here, we use HFA (instead of OCA) of Ref.[30] to study QDA nanowire with  $N=10$  because of its simplicity. Fig. 4 shows the  $G_e$ ,  $S$  and  $(ZT)_0$  as functions of temperature for various detuning energies ( $\Delta$ ). The other physical parameters are the same as those of Fig. 2. The behavior of  $G_e$  with respect to temperature can be understood by considering  $G_e \approx 1/(k_B T \cosh^2(\Delta/2k_B T))$  for  $U_\ell = 0$  (see the curve with triangle marks).  $S$  is proportional to  $T$  when temperature approaches zero (not shown here), whereas  $S \approx \Delta/k_B T$  at high temperatures and  $\Delta/\Gamma \gg 1$  (see the curves with triangle marks). In the absence of  $\kappa_{La}$ , a very large  $(ZT)_0$  appears in the low temperature regime. The maximum  $(ZT)_0$  is beyond three, which is a critical value for the realization of solid state coolers and power generators.  $(ZT)_0$  larger than 3 is a direct consequence of the fact  $G_e \gg \kappa_e$  ( $\kappa_e$  not shown here) and large enhancement of  $S^2$  in the Coulomb blockade regime. Using small nanowires in the quantum thermal conductance regime and a vacuum space to blockade surrounding phonon heat current was proposed to yield a vanishingly small phonon thermal conductivity.[33] However, such a design requires advanced nanotechnology. The results of Fig. 4(c) also imply that the on-site electron Coulomb interactions can be ignored only when  $U_\ell/k_B T \gg 1$ .  $(ZT)_0$  is highly overestimated at high temperatures in the absence of  $U_\ell$ .

Fig. 5(a) shows  $ZT$  in the presence of  $\kappa_{La}$  ( $\kappa_{La} = F_s \kappa_{ph}(A/L_x)$ ) for the case of a GaAs nanowire with  $L_z = L_y = 5 \text{ nm}$  and  $L_x = 250 \text{ nm}$ .  $F_s$  is assumed to be 0.1 in the calculation. The curves of Fig. 5(a) have one-to-one correspondence to those of Fig. 4(c). The maximum  $ZT$  value is significantly reduced in the presence of  $\kappa_{La}$ . This reduction of  $ZT$  results from the fact  $\kappa_{La} \gg \kappa_e$  [see Eq. (11)], which implies that the optimization of  $ZT$  can be achieved by reducing  $\kappa_{ph}$  and increasing power factor  $PF = S^2 G_e$  simultaneously. The maximum  $ZT$  depends on the detuning energy,  $\Delta$ . This behavior can be understood from the results of Fig. 3(d). The  $ZT$  value is almost independent of temperature for  $\Delta = 40\Gamma_0$ , when  $k_B T \geq 20\Gamma_0$ . This is because the ratio of  $G_e/(T\kappa_{La})$  is nearly constant. In the high temperature regime we have  $\kappa_{ph} \approx 1/T$  and  $G_e$  decays very slowly with increasing temperature.

Fig. 5(b) shows  $ZT$  as a function of temperature for various electron hopping strengths at  $\Delta = 40\Gamma_0$ .  $ZT$  is enhanced with increasing  $t_c$ . Under the condition  $\kappa_{La} \gg \kappa_e$ , the behavior of  $ZT$  with respect to  $t_c$  can be analyzed by the power factor  $PF = S^2 G_e$ . When the QD energy is far above  $E_F$  ( $\Delta = 40\Gamma_0$ ), the behavior of  $S = \Delta/k_B T$  is independent of  $t_c$  in the Coulomb blockade regime once  $k_B T \geq 10\Gamma_0$ . Therefore, the enhancement of  $ZT$  is completely determined by the increase of  $G_e$  with respect to  $t_c$ . When  $t_c$  is smaller than the tunneling

rate ( $\Gamma_L = \Gamma_R = \Gamma$ ),  $G_e$  increases quickly with increasing  $t_c$ , and it becomes insensitive to  $t_c$  when  $t_c \geq 2\Gamma_0$ . This demonstrates that the optimization of  $ZT$  can be realized by the enhancement of PF for a given  $\kappa_{La}$ .

In Fig. 5, we consider square nanowires with a small cross section with  $L_y = L_z = 5 \text{ nm}$ . To understand the dependence on QDA cross-sectional area, we show in Fig. 6  $ZT$  as a function of temperature for various values of  $L_z$  with  $L_y$  fixed at 5 nm. We adopt  $\Gamma_L = \Gamma_R = \Gamma = 3\Gamma_0$ ,  $t_c = 3.5\Gamma_0$ ,  $U_\ell = 30\Gamma_0$  and  $\Delta = 40\Gamma_0$ . In our model, we keep a large separation between QDAs along the z direction ( $D_s = 25 \text{ nm}$ ), this allow us to avoid the electron hopping effects and interdot Coulomb interactions between QDAs along that direction. Fig. 6 shows the maximum  $ZT$  of QDA with  $L_z = 7L_y$  can be larger than one. This is due to the enhancement of  $G_e$  with increased tunneling rates ( $\Gamma = 3\Gamma_0$ ). The  $ZT$  value reduces significantly for the cases with large  $L_z$  ( $\geq 13L_y$ ). This  $ZT$  reduction comes from the increased value of  $\kappa_{La}$  [see Fig. 1(b)]. If we reduce the separation,  $D_s$  between QDAs to increase the density of QDAs, the proximity effect arising from interdot Coulomb interactions between QDAs should be included.[33] In general, the proximity effect from interdot Coulomb interactions will suppress the  $G_e$  values.

#### IV. SUMMARY AND CONCLUSIONS

We have theoretically investigated the TE properties of QDAs embedded in nanowires connected to metallic electrodes in the Coulomb blockade regime. Both OCA and HFA calculations were examined. It was shown that HFA method gives unphysical results for the Seebeck coefficient at low temperature when the QDs are nearly half filled. However, it gives reasonable results at high temperatures when the QD energy levels are far above the Fermi level (low filling condition). Under the condition  $\kappa_{La} \gg \kappa_e$ , the optimization of  $ZT$  can be achieved by reducing  $\kappa_{La}$  and increasing the power factor  $PF = S^2 G_e$ , simultaneously. We found that for various design parameters,  $ZT > 1$  can be achieved. In our simulation, we assumed that the presence of QDs reduces the phonon conductivity in nanowires by a factor  $F_s = 0.1$ . It is conceivable that a smart nanostructure design which reduces the value of  $F_s$  further can increase the maximum  $ZT$  even more. The maximum  $ZT$  value of a QDA nanowire with small cross section is found insensitive to temperature variation (see Figs. 5(b) and 6). Such a feature is quite different from that of conventional thermoelectric materials.[1,2] The ability of QDAs to maintain  $ZT$  near its maximum value for a wide range of temperatures is an important feature in the realization of useful thermoelectric devices.[2]

#### Acknowledgments

This work was supported in part by the National Science Council of the Republic of China under Contract

Nos. NSC 103-2112-M-008-009-MY3 and NSC 101-2112-M-001-024-YM3.

\* E-mail:yiachang@gate.sinica.edu.tw

† E-mail address: mtkuo@ee.ncu.edu.tw

---

<sup>1</sup> A. J. Minnich, M. S. Dresselhaus, Z. F. Ren, and G. Chen, Energy Environ Sci **2** 466 (2009).

<sup>2</sup> M. Zebarjadi, K. Esfarjania, M.S. Dresselhaus, Z.F. Ren, and G. Chen, Energy Environ Sci **5** 5147 (2012).

<sup>3</sup> G. Mahan, B. Sales, and J. Sharp, Physics Today **50** (3) 42 (1997).

<sup>4</sup> R. Venkatasubramanian, E. Siivola, T. Colpitts, and B. O'Quinn, Nature **413** 597 (2001).

<sup>5</sup> A. I. Boukai, Y. Bunimovich, J. Tahir-Kheli, J. K. Yu, W. A. Goddard III, and J. R. Heath, Nature **451** 168 (2008).

<sup>6</sup> T. C. Harman, P. J. Taylor, M. P. Walsh, and B. E. LaForge, Science **297** 2229 (2002).

<sup>7</sup> K. F. Hsu, S. Loo, F. Guo, W. Chen, J. S. Dyck, C. Uher, T. Hogan, E. K. Polychroniadis, and M. G. Kanatzidis, Science **303** 818 (2004).

<sup>8</sup> M. S. Dresselhaus, G. Chen, M. Y. Tang, R. Yang, H. Lee, D. Wang, Z. Ren, J. P. Fleurial, and P. Gogna, Adv. Mater. **19**, 1043 (2007).

<sup>9</sup> David. M. T. Kuo, and Y. C. Chang, Nanotechnology **24**, 175403 (2013).

<sup>10</sup> P. Murphy, S. Mukerjee, and J. Moore, Phys. Rev. B **78**, 161406 (2008).

<sup>11</sup> Y. Dubi, and M. DiVentra, Phys. Rev. B, **79**, 081302 (2009).

<sup>12</sup> J. Liu, Q. F. Sun, and X. C. Xie, Phys. Rev. B **81**, 245323 (2010).

<sup>13</sup> M. Wierzbicki, and R. Swirkowicz, Phys. Rev. B **84**, 075410 (2011).

<sup>14</sup> D. Sanchez, and L. Serra, Phys. Rev. B **84**, 201307 (2011).

<sup>15</sup> P. Trocha, and J. Barnas, Phys. Rev. B **85**, 085408 (2012).

<sup>16</sup> D. M. T. Kuo, and Y. C. Chang, Phys. Rev. B **89**, 115416 (2014).

<sup>17</sup> M. G. Holland, Phys. Rev. **132**, 2461 (1963).

<sup>18</sup> H. Haug, and A. P. Jauho: Quantum Kinetics in Transport and Optics of Semiconductors (Springer, Heidelberg, 1996).

<sup>19</sup> David M. T. Kuo, and Y. C. Chang, arXiv:1209.0506.

<sup>20</sup> D. L. Nika, E. P. Pokatilov, A. A. Balandin, V. M. Fomin, A. Rastelli, and O. G. Schmidt, Phys. Rev. B **84**, 165415 (2011).

<sup>21</sup> G. Chen, and C. L. Tien, J. Thermophys. Heat Transfer **7**, 311 (1993).

<sup>22</sup> M. G. Holland, Phys. Rev. **134**, A471 (1964).

<sup>23</sup> D. Y. Li, Y. Y. Wu, P. Kim, L. Shi, P. D. Yang, and A. Majumdar, Appl. Phys. Lett. **83** 2934 (2003).

<sup>24</sup> A. I. Hochbaum, R. K. Chen, R. D. Delgado, W. J. Liang, E. C. Garnett, M. Najarian, A. Majumdar, and P. Yang, Nature **451**, 163 (2008).

<sup>25</sup> R. Chen, A. I. Hochbaum, P. Murphy, J. Moore, P. D. Yang, and A. Majumdar, Phys. Rev. Lett. **101**, 105501 (2008).

<sup>26</sup> G. Chen, J. Heat. Transfer **119**, 220 (1997).

<sup>27</sup> H. T. Chang, C. C. Wang, J. C. Hsu, M. T. Hung, P. W. Li, and S. W. Lee, Appl. Phys. Lett. **102**, 101902 (2013).

<sup>28</sup> C. C. Chen, Y. C. Chang, and D. M. T. Kuo, Phys. Chem. Chem. Phys. **17**, 6606 (2015).

<sup>29</sup> C. C. Chen, D. M. T. Kuo, and Y. C. Chang, Phys. Chem. Chem. Phys. accepted (2015), or arXiv: 1505.03944

<sup>30</sup> C. A. Stafford, D. M. Cardamone, and S. Mazumdar, Nanotechnolgy, **18**, 424014 (2007).

<sup>31</sup> J. P. Bergfield, and C. A. Stafford, Nano Letters **9** 3072 (2009).

<sup>32</sup> J. P. Bergfield, M. A. Solis, and C. A. Stafford, ACS Nano **4** 5314 (2010).

<sup>33</sup> D. M. T. Kuo, and Y. C. Chang, Phys. Rev. B **81**, 205321 (2010).

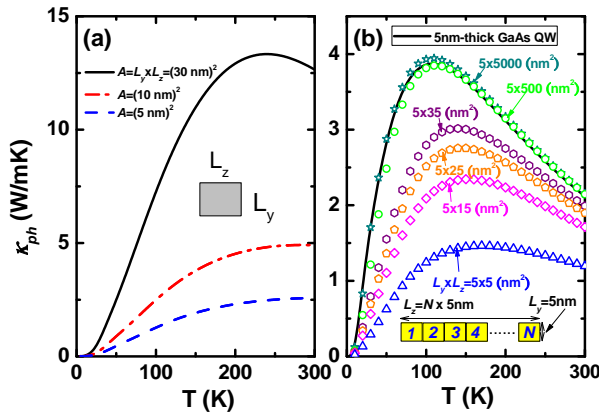


FIG. 1: (a) Phonon thermal conductivity of a silicon nanowire as a function of temperature for the different cross sections. The square cross section is defined as  $A = L_y \times L_z$ , where  $L_y$  and  $L_z$  are lateral sizes, and (b) phonon thermal conductivity of a GaAs nanowire with rectangular cross section  $A = L_y \times L_z$  as a function of temperature for different  $L_z$  values at fixed  $L_y = 5 \text{ nm}$ .

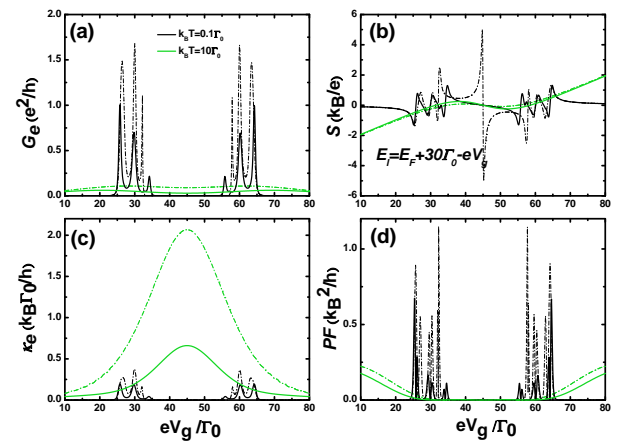


FIG. 2: (a) Electrical conductance ( $G_e$ ), (b) Seebeck coefficient ( $S$ ), (c) electron thermal conductance ( $\kappa_e$ ), and (d) power factor  $PF = S^2 G_e$  of triple QDs junction systems as a function of gate voltage for two different temperatures. Solid line and dot-dashed line are calculated by OCA and HFA, respectively.

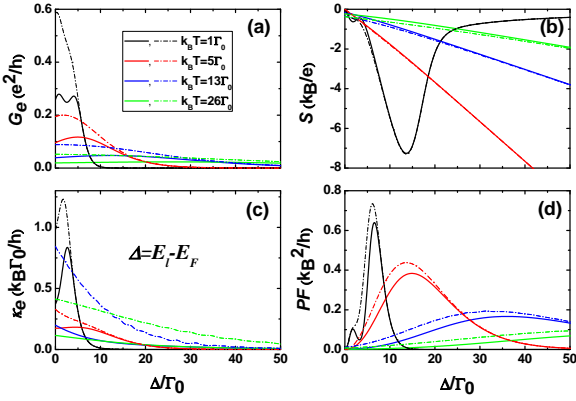


FIG. 3: (a) Electrical conductance ( $G_e$ ), (b) Seebeck coefficient ( $S$ ), (c) electron thermal conductance ( $\kappa_e$ ), and (d) power factor  $PF = S^2 G_e$  of triple QDs junction systems as a function of detuning energy  $\Delta = E_l - E_F$  for different temperatures. The other physical parameters are the same as those of Fig. 2.

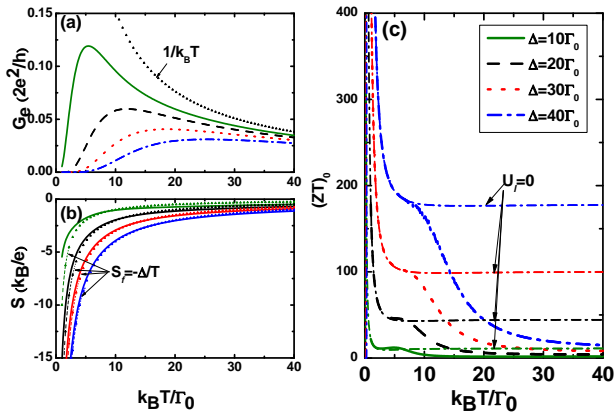


FIG. 4: (a) Electrical conductance, (b) Seebeck coefficient and (c)  $(ZT)_0$  of a QDA system with dot number  $N=10$  in the absence of  $\kappa_{ph}$  as a function of temperature for different detuned energies. Other physical parameters are the same as those of Fig.2.

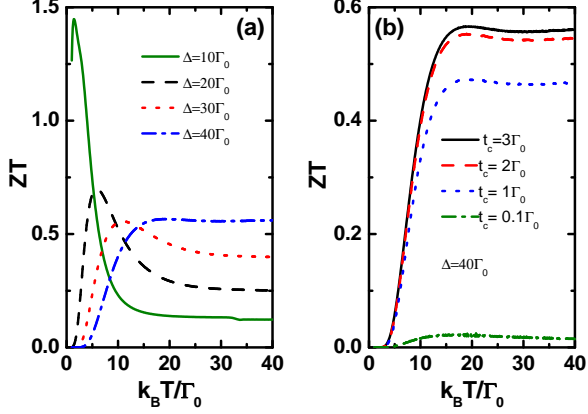


FIG. 5: Figure of merit of a QDA system with dot number  $N=10$  in the presence of  $\kappa_{ph}$  as a function of temperature. The curves of diagram (a) correspond to those of Fig. 4. Diagram (b) shows  $ZT$  for various electron hopping strengths.

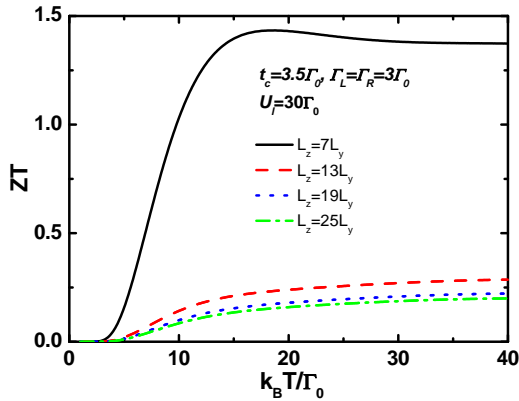


FIG. 6:  $(ZT)$  as a function of temperature for different  $L_z$  values. The physical parameters are  $t_c = 3.5\Gamma_0$  and  $\Gamma_L = \Gamma_R = 3\Gamma_0$ . Solid line ( $L_z = 7L_y$ ), dashed line ( $L_z = 13L_y$ ), dotted line ( $L_z = 19L_y$ ) and dot-dashed line ( $L_z = 25L_y$ ). Other physical parameters are the same as those of Fig. 5(b).